Anomalous optical drag

Chitram Banerjee,[1] Yakov Solomons,[1] A. Nicholas Black ⬤,[2,*] Giulia Marcucci ⬤,[3] David Eger,[1] Nir Davidson,[1]
Ofer Firstenberg ⬤,[1] and Robert W. Boyd ⬤[2,3,4]

[1]*Department of Physics of Complex Systems, Weizmann Institute of Science, Rehovot 76100, Israel*
[2]*Department of Physics and Astronomy, University of Rochester, Rochester, New York 14627, USA*
[3]*Department of Physics, University of Ottawa, Ottawa, Canada ON K1N 6N5*
[4]*Institute of Optics, University of Rochester, Rochester, New York 14627, USA*

A moving dielectric medium can displace the optical path of light passing through it, a phenomenon known as the Fresnel-Fizeau optical drag effect. The resulting displacement is proportional to the medium's velocity. In this paper, we report on the observation of an anomalous optical drag effect, where the displacement is still proportional to the medium's speed but along the direction opposite to the medium's movement. We conduct an optical drag experiment under conditions of electromagnetically induced transparency and observe the transition from normal, to null, to anomalous optical drag by modification of the two-photon detuning.

I. INTRODUCTION

As light travels through a moving medium, it is dragged along the axis of the medium's motion. This effect, known as optical drag, was first described theoretically by Fresnel in 1818 [1,2]. In 1851, Fizeau demonstrated Fresnel's drag experimentally [3]. However, Fresnel and Fizeau ignored the effect of refractive index dispersion. This effect was incorporated by Lorentz, who in 1904 predicted the influence of dispersion on the optical drag effect for a moving medium with a fixed boundary [4]. Four years later, Laub developed a theoretical treatment for optical drag in a dispersive moving medium with a moving boundary [5]. Many experiments that measured the effect of dispersion on optical drag were then reported by Zeeman and coworkers [6–10]. They measured the wavelength dependence of optical drag in water [6,7] and performed other experiments to measure optical drag in quartz and flint glass [8–10] where dispersion was found to have a significant effect on optical drag.

The transverse displacement of a light beam experiencing optical drag depends on both the refractive and group indices of the beam in the moving medium [11]. It is well known that materials can be highly dispersive under nearly resonant excitation [12]. This large dispersion leads to a large group index and thus to highly subluminal pulse propagation (sometimes referred to as slow light). Consequently, the optical drag effect is enhanced notably [13,14]. Since absorption is typically high under nearly resonant excitation, most observations of slow light have relied upon electromagnetically induced transparency (EIT) [15,16] or coherent population oscillation [17–19]. These effects have the added benefit of providing very narrow resonances, leading to high dispersion and large group indices. As a result, EIT has been used to further enhance the optical drag effect [20] and perform high precision velocimetry [21].

Under conditions of anomalous dispersion, the group index can become negative, leading to one manifestation of the so-called fast light effect, where the peak of a pulse exits the medium before it has entered [22]. After the pulse has exited the medium, its peak is shifted forward relative to an identical pulse that has passed through vacuum. Under certain circumstances, the advancement of the peak can be attributed to pulse reshaping caused by saturated absorption or gain [23,24].

In this paper, we report on the anomalous optical drag effect, where the light beam shifts in the direction opposite to the motion of the medium. We excite EIT in a moving cell of rubidium vapor and induce a transition from normal to anomalous optical drag by properly modifying the two-photon detuning. We report here an experimental demonstration of anomalous transverse drag; anomalous longitudinal drag has been reported recently [25].

Despite the connection between anomalous dispersion and anomalous drag, we find the latter quite nontrivial. In the normal drag regime, the picture of a slow-light polariton, which is dragged by the moving atoms that comprise it, intuitively holds. In the anomalous drag regime, however, this picture completely breaks down. The beam moves in the opposite direction to the atoms and, in fact, moves even further away when the atoms move faster. Moreover, negative drag can provide much needed insight on paradoxical scenarios such as negative tunneling times [26], superluminal light propagation [27–29], and negative dwell times [30].

II. THEORETICAL MODEL

The transverse Fresnel-Fizeau drag effect in a generic dispersive medium has been treated theoretically by starting from the linearized Lorentz transformation for the frequency

---

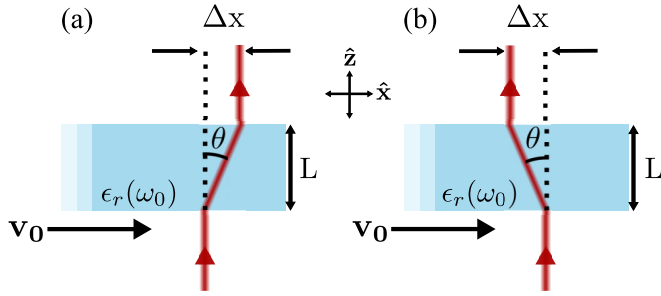*Corresponding author: ablack18@ur.rochester.edu

FIG. 1. Pictorial representation of the transverse Fresnel-Fizeau drag effect for (a) normal optical drag and (b) anomalous optical drag.

and wave vector of a beam propagating inside a moving medium [11]. Let us consider a nonmagnetic and isotropic medium (i.e., relative magnetic permeability $\mu = 1$ and dielectric tensor $\epsilon_{ij} = \epsilon \delta_{ij}$), with $\epsilon_r = \mathrm{Re}[\epsilon]$. As shown in Fig. 1(a), if the medium is moving with velocity $\boldsymbol{v_0} = v_0 \hat{\boldsymbol{x}}$, where z is the longitudinal and x, y are the transverse coordinates, the probe light beam experiences a shift along x of

$$\Delta x = L \tan \theta. \tag{1}$$

In Eq. (1), L is the medium's longitudinal length, and θ the light's walk-off angle inside the medium, with

$$\tan \theta = \frac{v_0}{c}\left(\frac{c}{v_g} - \frac{v_p}{c}\right), \tag{2}$$

where c is the speed of light in vacuum [11]. The group velocity and phase velocity of light in the medium are

$$v_g = \frac{c}{\sqrt{\epsilon_r(\omega_0)} + \frac{\omega_0}{2\sqrt{\epsilon_r(\omega_0)}}\left(\frac{d\epsilon_r}{d\omega}\right)_{\omega_0}}, \tag{3}$$

$$v_p = \frac{c}{\sqrt{\epsilon_r(\omega_0)}}, \tag{4}$$

respectively.

Equation (2) can be expressed in terms of the medium's refractive index $n(\omega) = \sqrt{\epsilon_r(\omega)}$, or after fixing the value of the carrier frequency, as $n_0 = \sqrt{\epsilon_r(\omega_0)}$. Equations (3) and (4) can then be rewritten as $v_g = c/n_{g,0}$ and $v_p = c/n_0$, where $n_{g,0} = n_0 + (\omega \frac{dn}{d\omega})_{\omega_0}$ is the group index. The resulting expression,

$$\tan \theta = \frac{v_0}{c}\left(n_{g,0} - \frac{1}{n_0}\right), \tag{5}$$

reveals the existence of three different regimes: (i) $n_{g,0} > n_0^{-1}$ normal (or positive) optical drag [Fig. 1(a)], (ii) $n_{g,0} = n_0^{-1}$ absence of optical drag, and (iii) $n_{g,0} < n_0^{-1}$ anomalous (or negative) optical drag [Fig. 1(b)].

For a beam experiencing normal dispersion, if $v_p \approx c$ and $v_g \ll c$, the drag can be approximated in terms of the group delay, τ: $\Delta x \approx L v_0 / v_g = \tau v_0$ [20]. The conditions of anomalous dispersion, $n_{g,0} < 0$, satisfy regime (iii), hence the name *anomalous* drag. In highly dispersive conditions, the relation $\Delta x \approx \tau v_0$ is still valid because $n_{g,0}$ is negative and $|n_{g,0}| \gg 1$.

In EIT, the transition from normal to anomalous drag occurs close to the transition from negative to positive two-photon detuning, δ. To model optical drag under EIT conditions, we begin from Eq. (50) in [15], which describes the steady-state propagation of a probe beam under EIT in a gaseous medium of diffusing atoms. The medium's velocity, $\boldsymbol{v_0}$, is accounted for by adding a nonzero mean to the Boltzmann distribution of atomic velocities with thermal velocity $v_{\mathrm{th}} = (k_B T / m)^{1/2}$:

$$F(\boldsymbol{v}) = \frac{\exp\left(-\frac{(\boldsymbol{v}-\boldsymbol{v_0})^2}{2v_{\mathrm{th}}^2}\right)}{2\pi v_{\mathrm{th}}^2}. \tag{6}$$

k_B is the Boltzmann constant, T is the temperature, and m is the atomic mass. Assuming negligible diffraction, the dynamics of the probe beam are described by

$$[-i\delta + \gamma + K|\tilde{\Omega}_2(\boldsymbol{r})|^2 - D(\partial_{\boldsymbol{r}} - i\boldsymbol{\Delta q})^2 + (\partial_{\boldsymbol{r}} - i\boldsymbol{\Delta q})\cdot\boldsymbol{v_0}][\alpha\tilde{\Omega}_2(\boldsymbol{r})]^{-1}(\partial_z + \alpha)\tilde{\Omega}_1(\boldsymbol{r}) = K\tilde{\Omega}_2^*(\boldsymbol{r})\tilde{\Omega}_1(\boldsymbol{r}). \tag{7}$$

Here, $\tilde{\Omega}_{1,2}$ represent the Rabi frequency envelopes in the slowly varying envelope approximation for the probe and control beams, respectively, and K is the one-photon complex spectrum with total linewidth Γ incorporating homogeneous dephasing and Doppler broadening of the optical transition. Moreover, γ is the decoherence rate of the ground-state transition, D is the spatial diffusion coefficient, $\boldsymbol{\Delta q} = \boldsymbol{q}_2 - \boldsymbol{q}_1$ is the probe-control wave-vector mismatch (with absolute value Δq along $\hat{\boldsymbol{x}}$), and α is the attenuation (per unit distance) without EIT.

In Fourier space, stressing that the medium velocity is parallel to the x axis, one obtains

$$\partial_z \Omega_1 = i\frac{k_z}{2}\chi(k_x, k_z, \delta)\Omega_1 \tag{8}$$

with the susceptibility derived from Eq. (7):

$$\chi(k_x, k_z, \delta) = i\frac{2\alpha}{k_z}\left[1 - \frac{K|\Omega_2|^2}{-i\delta + \gamma + K|\Omega_2|^2 + D(k_x + \Delta q)^2 - i(k_x + \Delta q)v_0}\right]. \tag{9}$$

The probe susceptibility's dependence on k_z is such that $\partial_{k_z}[k_z\chi(k_x, k_z, \delta)] = 0$. It should be noted that Eq. (8) is exact only when the control field is an infinite plane wave, $\Omega_2(\boldsymbol{r}) = \Omega_2$. Nonetheless, quantitative agreement between

Eq. (8) and experiment can be achieved using a control field of finite extent as long as its beam waist, w_0, is wide enough to satisfy $w_0 \gg \max\{\sqrt{D\tau}, v_0\tau\}$ [20].
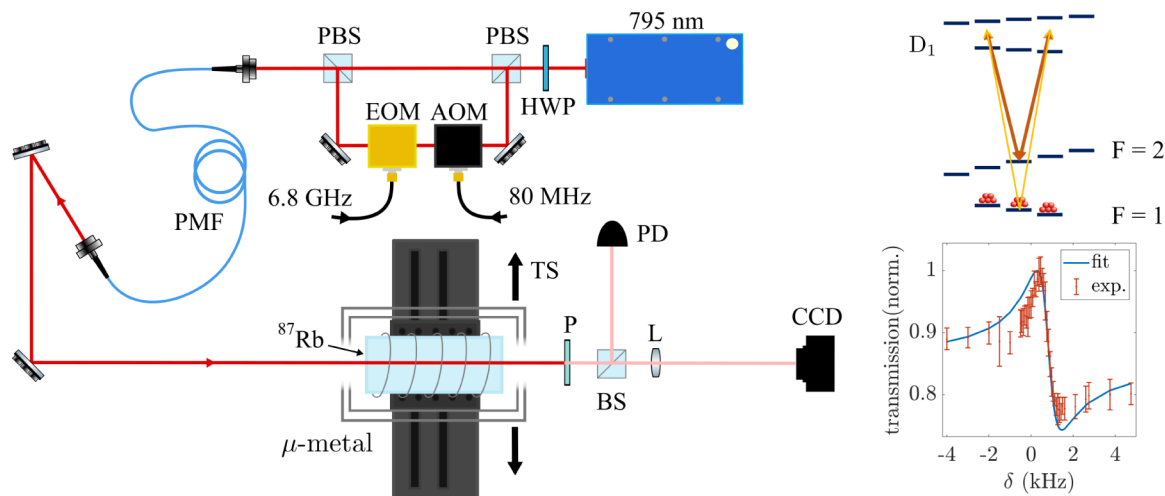
FIG. 2. Experimental setup for observing anomalous optical drag under conditions of EIT. Left: The probe and control fields are derived from a diode laser (795 nm) tuned to the D_1 transition in ^{87}Rb. A half-wave plate (HWP) controls the relative power of the orthogonally polarized probe and control fields before they are split by a polarizing beamsplitter. The probe passes through an electro-optic modulator (EOM) and an acousto-optic modulator (AOM) to tune it to the $F = 1 \rightarrow F' = 1, 2$ transition and vary the two-photon detuning, δ, respectively. The probe and control are then recombined at a PBS before being coupled into a single-mode polarization-maintaining fiber (PMF). After exiting the PMF, both fields pass through a ^{87}Rb cell that is shielded from stray magnetic fields by a double-layer magnetic shield (μ metal). A solenoid creates a uniform magnetic field to lift the degeneracy of the Zeeman sublevels. The probe and control fields interact through an EIT scheme shown in the upper right panel. The dominant interaction occurs around the $m_F = 0 \longrightarrow m'_F = \pm1$ transitions for the probe (yellow arrows) and control (brown arrows). By detuning both the probe and control -250 MHz below the $F' = 2$ excited state, the two-photon line shape is sufficiently asymmetric to produce anomalous dispersion (lower right panel) [31]. The normalized transmission using the model of Eq. (9) was fit to the transmission data simultaneously to all other data sets using Γ, γ, and Δq as free parameters. The entire Rb cell apparatus is mounted on a translation stage (TS) that travels transverse to the beam propagation. A polarizer (P) after the cell filters out the control field, and the probe field is split into two paths by a beamsplitter (BS). One path terminates on a photodiode (PD) for measuring the group delay of the probe. In the other, a lens (L) images the output facet of the cell onto a camera (CCD).

The resulting solution of Eq. (7) is

$$\tilde{\Omega}_1(x, z) = \mathcal{F}^{-1}\left\{ \mathcal{F}[\tilde{\Omega}_1|_{z=0}] \exp\left[i\frac{\chi(k_x, k_z, \delta)}{2} k_z z \right] \right\}, \quad (10)$$

where $\mathcal{F}$ is the Fourier-transform operator.

This picture furnishes an expression for the transverse shift in Eq. (1), where the dependence of the optical drag and group delay on the two-photon detuning appears explicitly [20]:

$$\Delta x = \partial_{k_x} \text{Re}\left(\frac{\chi(k_x, k_z, \delta)}{2} k_z L \right), \quad (11)$$

$$\tau = \partial_\delta \text{Re}\left(\frac{\chi(k_x, k_z, \delta)}{2} k_z L \right). \quad (12)$$

III. EXPERIMENTAL RESULTS

The experimental arrangement for measuring anomalous optical drag is shown in Fig. 2. The control and probe beams are obtained from the same diode laser, the center frequency of which is set to 795 nm to excite the D_1 transition of the ^{87}Rb atoms. The probe is tuned to the $F = 1 \rightarrow F' = 1, 2$ transition, and the control is tuned to the $F = 2 \rightarrow F' = 1, 2$ transition. The probe and control beams exit the same polarization-maintaining fiber with a radius $w_p = w_c = 2$ mm. The total control power is $\approx 40\,\mu$W and that of the probe is $\approx 2\,\mu$W. The ^{87}Rb vapor is kept in a magnetically shielded Pyrex cell of length $L = 7.5$ cm. The

cell contains buffer gases N_2 (10 Torr) and Ar (90 Torr) and is heated to $55\,^{\circ}$C, in which case the thermal motion of the atoms behaves diffusively with a diffusion coefficient of $D \approx 166$ mm^2/s. The cell assembly is mounted on a Thorlabs DDSM100 motorized stage, so it can move with a constant velocity while crossing the beams. By comparing the center of mass of the probe beam's transverse profile when the cell is moving and not moving, the transverse drag is obtained. The dependence of optical drag on the two-photon detuning is shown in Fig. 3. Both Δx and τv_0 are measured at cell velocities of 200 mm/s (a) and -200 mm/s (b), the maximum achievable velocities of our system. The models of Eqs. (11) and (12) are fit to the Δx and τv_0 data, respectively, using maximum likelihood estimation with three free parameters: Γ, γ, and Δq. Furthermore, we assume that the data have Gaussian random errors. The likelihood function was composed of the data in Figs. 3 and 4 and the transmission data in the inset of Fig. 2, along with their corresponding models [Eqs. (11), (12), and (9), respectively] and uncertainties. Thus, we obtained values of the three fit parameters that describe all data sets: $\Gamma = 266(2)$ MHz, $\gamma = 145(2)$ Hz, and $\Delta q = 1.2(3) \times 10^{-6}\, 2\pi/\lambda$. Uncertainties in the fit parameter values were obtained through Monte Carlo simulation. The data show a strong dependence on the two-photon detuning δ; normal optical drag occurs for $\delta < 425$ Hz, while anomalous optical drag occurs for $\delta > 425$ Hz and peaks around $\delta = 900$ Hz. Note that the τv_0 data predict approximately half as much optical drag than is actually measured, Δx. The
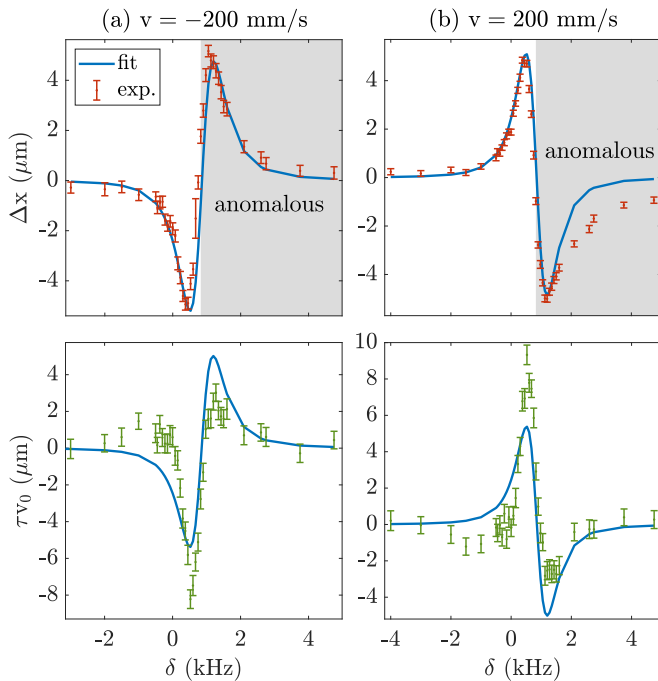
FIG. 3. Dependence of optical drag on two-photon detuning δ. Top row: The measured transverse beam displacement Δx is in the same direction as the velocity of the cell on the red-detuned side of the two-photon transition and in the opposite direction on the blue-detuned side. This behavior is observed for both (a) negative and (b) positive cell velocities. Bottom: There are deviations of up to a factor of 2 between the measured τv_0 and Δx, potentially due to higher-order dispersion combined with the finite temporal duration of the probe. The fit lines are obtained from maximum likelihood estimation using the models of Eqs. (11) and (12) with Γ, γ, and Δq as free parameters. The difference between the error bars' lengths in the top row of (a) and (b) is due to difference in the mechanical precision of the translation stage for these two trajectories. An offset of 425 Hz is added to the fit lines to account for a systematic error in the detuning measurement.
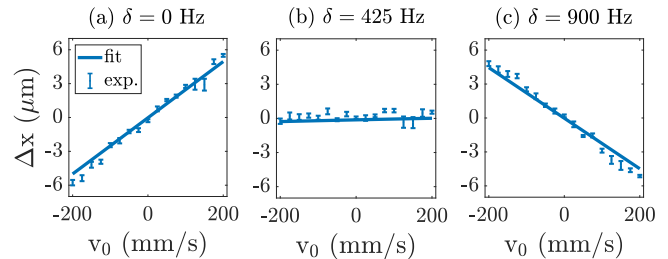

FIG. 4. Experimental observation of optical drag at various dragging velocities. (a) At a two-photon detuning of $\delta = 0$ Hz the beam experiences normal optical drag. The dependence of the drag on the velocity is approximately linear from $v_0 = -200$ to 200 mm/s. (b) There is effectively no optical drag for any cell velocity when $\delta = 425$ Hz. (c) At $\delta = 900$ Hz the beam undergoes anomalous optical drag for all velocities in the domain $v_0 = -200$ to 200 mm/s. The fit lines were obtained by fitting Eq. (11) to all data sets simultaneously.

breakdown of this approximation may result from higher-order derivatives of the spectral response at the transition from normal to anomalous dispersion. These effects are present for finite duration pulses, like those used in this experiment.

Figure 4 shows the dependence of optical drag on dragging velocity. Despite the nonlinear dependence of Eq. (9), and consequently Eq. (11), on the dragging velocity, the data are approximately linear in this experimental regime. Interestingly, for a two-photon detuning of $\delta = 425$ Hz, almost no optical drag is present for any dragging velocity, as shown in Fig. 4(b). The null optical drag is unique and corresponds to conditions of zero group delay in the medium (zero crossing in Fig. 3). Normal [Fig. 4(a)] and anomalous [Fig. 4(c)] drags are observed over a range of velocities with a high degree of symmetry between the normal and anomalous effects.

IV. CONCLUSIONS

We demonstrated normal, null, and anomalous optical drag effects experimentally and modeled them theoretically. By using EIT in ^{87}Rb vapor, we were able to maximize the

dispersion and minimize the loss associated with near-resonant atomic excitation. While the scientific community has already reported on the normal drag effect in the last two decades [11,13,14,20], as well as the anomalous longitudinal drag effect [25], here we report our observation of anomalous transverse drag. Our measurements showed that the beam's displacement is proportional to the velocity of the medium through which it passes, with a direction depending on the sign of the medium's dispersion. For positive group delays, the beam experiences normal optical drag and is dragged in the direction of the material motion. When the measured group delay is negative, the beam is dragged in a direction opposite to the material displacement. In a regime where the group index is exactly equal to the inverse of the refractive index and there is no measured group delay, there is no optical drag at any material velocity.

In the gaseous system we study, one can generate nontrivial velocity patterns, such as vortices and linear velocity gradients. Under slow-light conditions, a vortex is expected to rotate the optical field [13], while a linear velocity gradient will lead to an angular deflection of the beam in the direction of the gradient. These manipulations, combined with linear drag, can be externally controlled at a high rate by tuning the frequency of the control field and thus could have potential applications in ultrafast beam shaping and steering. Conversely, the overall transformation of an incoming light field can be used to directly and quantitatively probe nontrivial velocity fields [32]. These include intricate flow patterns and transient gradients, for example, in gas lasers [33] or on moving, accelerating platforms. Alternating between normal and anomalous drag in these types of sensors and monitoring the difference signal can be advantageous for subtracting any nonatomic effect and removing systematic errors.

Furthermore, the average velocity of the atoms, due to the motion of the cell or the macroscopic flow, adds to their underlying thermal velocity distribution, resulting in a drift-diffusive atomic motion. When atomic diffusion is significant, it may lead to paraxial diffusion of the light field [34,35] and also, similarly to anomalous and null drag, to effective paraxial diffraction that eliminates and even reverses the free-space optical diffraction [36].

[1] A. J. Fresnel, Letter from Mr. Fresnel to Mr. Arago, on the influence of earthly movement in some optical phenomena, Ann. Chim. Phys. **9**, 57 (1818).

[2] K. F. Schaffner, in *Nineteenth-Century Aether Theories*, The Commonwealth and International Library: Selected Readings in Physics, 1st ed. (Pergamon, Oxford, 1972).

[3] M. H. Fizeau, Hypotheses relating to the luminous ether and on an experiment which appears to demonstrate that the motion of bodies changes the speed with which light propagates in their interior, C. R. Acad. Sci. **33**, 349 (1851).

[4] H. A. Lorentz, Electromagnetic phenomena in a system moving with any velocity smaller than that of light, Proc. KNAW **6**, 809 (1904).

[5] J. Laub, To the optics of moving bodies, Ann. Phys. (NY) **330**, 175 (1908).

[6] P. Zeeman, Fresnel's coefficient for light of different colors (first part), Proc. KNAW **17**, 445 (1914).

[7] P. Zeeman, Fresnel's coefficient for light of different colors (second part), Proc. KNAW **18**, 398 (1915).

[8] P. Zeeman, The propagation of light in moving transparent solid substances. I. Apparatus for the observation of the Fizeau-effect in solid substances, Proc. KNAW **22**, 462 (1919).

[9] A. Snethlage and P. Zeeman, The propagation of light in moving, transparent, solid substances. II. Measurement of the Fizeau effect in quartz, Proc. KNAW **22**, 512 (1920).

[10] P. Zeeman, W. D. Groot, A. Snethlage, and G. C. Dibbetz, The propagation of light in moving, transparent, solid substances. III. Measurements on the Fizeau effect in flint glass, Proc. KNAW **23**, 1402 (1922).

[11] I. Carusotto, M. Artoni, G. C. La Rocca, and F. Bassani, Transverse Fresnel-Fizeau drag effects in strongly dispersive media, Phys. Rev. A **68**, 063819 (2003).

[12] R. W. Boyd, *Nonlinear Optics*, 4th ed. (Academic, New York, 2020).

[13] S. Franke-Arnold, G. Gibson, R. W. Boyd, and M. J. Padgett, Rotary photon drag enhanced by a slow-light medium, Science **333**, 65 (2011).

[14] A. Safari, I. De Leon, M. Mirhosseini, O. S. Magaña-Loaiza, and R. W. Boyd, Light-Drag Enhancement by a Highly Dispersive Rubidium Vapor, Phys. Rev. Lett. **116**, 013601 (2016).

[15] O. Firstenberg, M. Shuker, R. Pugatch, D. R. Fredkin, N. Davidson, and A. Ron, Theory of thermal motion in electromagnetically induced transparency: Effects of diffusion, Doppler broadening, and Dicke and Ramsey narrowing, Phys. Rev. A **77**, 043830 (2008).

[16] O. Firstenberg, M. Shuker, N. Davidson, and A. Ron, Elimination of the Diffraction of Arbitrary Images Imprinted on Slow Light, Phys. Rev. Lett. **102**, 043601 (2009).

[17] M. S. Bigelow, N. N. Lepeshkin, and R. W. Boyd, Superluminal and slow light propagation in a room-temperature solid, Science **301**, 200 (2003).

[18] M. S. Bigelow, N. N. Lepeshkin, and R. W. Boyd, Observation of Ultraslow Light Propagation in a Ruby Crystal at Room Temperature, Phys. Rev. Lett. **90**, 113903 (2003).

[19] G. Piredda and R. W. Boyd, Slow light by means of coherent population oscillations: Laser linewidth effects, J. Eur. Opt. Soc. **2**, 07004 (2007).

[20] Y. Solomons, C. Banerjee, S. Smartsev, J. Friedman, D. Eger, O. Firstenberg, and N. Davidson, Transverse drag of slow light in moving atomic vapor, Opt. Lett. **45**, 3431 (2020).

[21] Z. Chen, H. M. Lim, C. Huang, R. Dumke, and S.-Y. Lan, Quantum-Enhanced Velocimetry with Doppler-Broadened Atomic Vapor, Phys. Rev. Lett. **124**, 093202 (2020).

[22] R. W. Boyd, Slow and fast light: Fundamentals and applications, J. Mod. Opt. **56**, 1908 (2009).

[23] N. G. Basov, R. V. Ambartsumyan, V. S. Zuev, P. G. Kryukov, and V. S. Letokhov, Propagation velocity of an intense light pulse in a medium with inverse population, Sov. Phys. Dokl. **10**, 1039 (1966).

[24] N. G. Basov, R. V. Ambartsumyan, V. S. Zuev, P. G. Kryukov, and V. S. Letokhov, Nonlinear amplification of light pulses, Sov. Phys. JETP **23**, 16 (1966).

[25] T. Qin, J. Yang, F. Zhang, Y. Chen, D. Shen, W. Liu, L. Chen, X. Jiang, X. Chen, and W. Wan, Fast- and slow-light-enhanced light drag in a moving microcavity, Commun. Phys. **3**, 118 (2020).

[26] X. Gutiérrez de la Cal, M. Alkhateeb, M. Pons, A. Matzkin, and D. Sokolovski, Klein paradox for bosons, wave packets and negative tunnelling times, Sci. Rep. **10**, 19225 (2020).

[27] R. Arun, Superluminal light propagation via quantum interference in decay channels, Phys. Rev. A **94**, 043843 (2016).

[28] Z. A. Sabegh and M. Mahmoudi, Superluminal light propagation in a normal dispersive medium, Opt. Express **29**, 20463 (2021).

[29] L. J. Wang, A. Kuzmich, and A. Dogariu, Gain-assisted superluminal light propagation, Nature (London) **406**, 277 (2000).

[30] J. Sinclair, D. Angulo, K. Thompson, K. Bonsma-Fisher, A. Brodutch, and A. M. Steinberg, Measuring the time atoms spend in the excited state due to a photon they do not absorb, PRX Quantum **3**, 010314 (2022).

[31] E. E. Mikhailov, V. A. Sautenkov, I. Novikova, and G. R. Welch, Large negative and positive delay of optical pulses in coherently prepared dense Rb vapor with buffer gas, Phys. Rev. A **69**, 063808 (2004).

[32] W. Merzkirch, *Flow Visualization*, 2nd ed. (Academic, New York, 1987), Chap. 3, pp. 115–231.

[33] E. Yacoby, K. Waichman, O. Sadot, B. D. Barmashenko, and S. Rosenwaks, Flowing-gas diode pumped alkali

lasers: Theoretical analysis of transonic vs supersonic and subsonic devices, Opt. Express **24**, 5469 (2016).

[34] O. Firstenberg, M. Shuker, A. Ron, and N. Davidson, Colloquium: Coherent diffusion of polaritons in atomic media, Rev. Mod. Phys. **85**, 941 (2013).

[35] O. Firstenberg, P. London, D. Yankelev, R. Pugatch, M. Shuker, and N. Davidson, Self-Similar Modes of Coherent Diffusion, Phys. Rev. Lett. **105**, 183602 (2010).

[36] O. Firstenberg, P. London, M. Shuker, A. Ron, and N. Davidson, Elimination, reversal and directional bias of optical diffraction, Nat. Phys. **5**, 665 (2009).